Journal of the European Ceramic Society 36 (2016) 2363–2369

Contents lists available at www.sciencedirect.com

Journal of the European Ceramic Society

journal homepage: www.elsevier.com/locate/jeurceramsoc

Fast and large area fabrication of hierarchical bioinspired superhydrophobic silicon surfaces

Simone Ghio[a,b], Giovanni Paternoster[b], Ruben Bartali[b], Pierluigi Belluti[b], Maurizio Boscardin[b,**], Nicola M. Pugno[a,b,c,*]

[a] Laboratory of Bio-inspired & Graphene Nanomechanics, Department of Civil, Environmental and Mechanical Engineering, University of Trento, Via Mesiano 77, 38123 Trento, Italy
[b] Center for Materials and Microsystems, Fondazione Bruno Kessler, Via Sommarive 18, 38123 Povo, TN, Italy
[c] School of Engineering and Materials Science, Queen Mary University of London, Mile End Road, London E1 4NS, UK

ARTICLE INFO

Article history:
Received 9 December 2015
Received in revised form 18 January 2016
Accepted 27 January 2016
Available online 8 February 2016

Keywords:
Bioinspired
Hierarchical Structures
Superhydrophobic
Silicon Oxide
Micro-fabrication

ABSTRACT

In this work we present a new method to generate hierarchical surfaces, inspired by lotus leaf, on a silicon substrate. Mimicking leafs with particular properties, such as low adhesion, water repellence and self-cleaning, is an interesting case of study in the branch of bioinspired materials. These properties arise from a combination of surface chemistry and topography. The lotus leaf surface exhibits a highly controlled specific roughness, which has been studied and imitated by several researchers. The great challenge that has still to be solved is to reproduce lotus-inspired surfaces rapidly and on large areas. Our method consists in a combination of wet and dry etch with soft lithography, able to generate nano- and micro-hierarchical structures on silicon surfaces. Two different kinds of hierarchical structures are generated by changing the order of the etch steps. The surfaces generated were then characterized by measuring both the contact angle and the sliding angle. Finally, to validate experimental results, analytical models were implemented to predict the contact angle. The best surface displayed wetting performances superior even to those of the natural lotus leaf, thanks to the hierarchical structure, with a contact angle of 171° and a tilt angle of 4° with production time of about 90 min per silicon wafer, or 30 s/cm^2.

1. Introduction

Hierarchical structures such as the ones found on the lotus leaf [1,2], are useful to improve water repellence of a surface. Specific roughness topologies are in general able to change the wetting property of a surface [3,4]. Different studies demonstrate theoretically [5–7] and experimentally [8,9] the importance of hierarchy. In order to generate hierarchical structures different processes have already been proposed in the literature, typically having in common rather long and complex fabrication processes [8,10,11].

The aim of this work is to fabricate hierarchical silicon surfaces with a new and fast method applicable to large areas.

The method presented, in this paper is a highly accurate, fast and repeatable microfabrication process for producing superhydrophobic surfaces. It combines an anisotropic wet etch in a solution based on Tetramethylammonium hydroxide (TMAH) [12] and a dry etching. The process herein described requires a minimum 7-min TMAH processing step plus 9-min of dry etching. Depending on the desired height of the pillars, the maximum processing time is no more than a few hours.

In Section 2 a description of how the silicon-based micro-nano textured and hierarchical structures were fabricated is reported. Two different base patterns were used: square-base or hexagonal-base patterns. Structures without hierarchy were fabricated and used as reference structures in wettability tests. Structures are formed by pillars with different diameters and pitch distances; Fig. 1 illustrates the geometries that were fabricated. Surfaces were tested for static contact angle and tilt angle. The flat surfaces and the textured ones were also tested. Results show how these rapidly generated large surfaces display wetting performances superior even than those of the natural lotus leaf, also thanks to hierarchy.

In Section 3 an analytical model, based on Wenzel and Cassie–Baxter models, is implemented to validate the experimental

* Corresponding author at: Laboratory of Bio-inspired & Graphene Nanomechanics, Department of Civil, Environmental and Mechanical Engineering, University of Trento, Via Mesiano 77, 38123 Trento, Italy.
** Corresponding author at : Center for Materials and Microsystems, Fondazione Bruno Kessler, Via Sommarive 18, 38123 Povo, TN, Italy
E-mail addresses: boscardi@fbk.eu (M. Boscardin), nicola.pugno@unitn.it (N. M. Pugno).

http://dx.doi.org/10.1016/j.jeurceramsoc.2016.01.041
0955-2219/

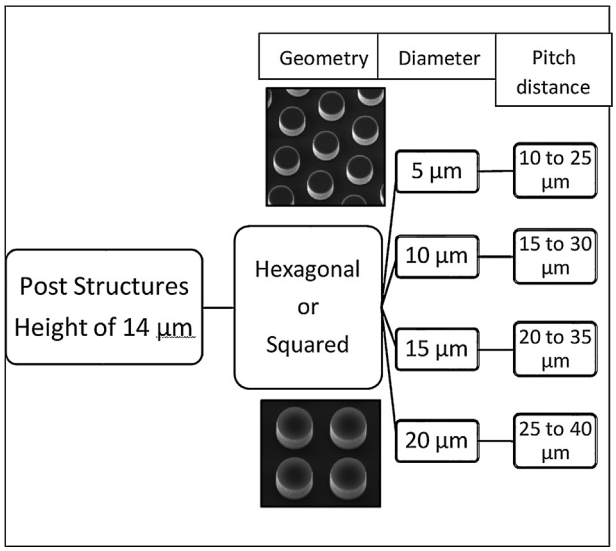

Fig. 1. Sizes and shapes of realized structures.

results and to find the most suitable conditions for water-surface interaction for future designs. Sections 4 and 5 close the article with the discussion of the results and the conclusions.

2. Experimental analysis

In this section the experimental part of the work is presented. First, the methods used to generate the surfaces are described, and then the wetting characterizations, for both non-hierarchical and hierarchical structures, are reported.

2.1. Surface generation

All the patterns and structures presented in this work were fabricated using a standard CMOS-like process. Post structures were fabricated using a lithographic step followed by dry etching. The dry etching was performed with Deep Reactive Ion Etching (DRIE) equipment, Alcatel AMS 1000.

The sizes and shapes of post structures are summarized in Fig. 1. Each patter presents pillars with different diameters and pitch distances. Diameter goes from 5 μm up to 20 μm, in steps of 5 μm and for each value four different pitch distances were considered, from 10 μm up to 40 μm. Furthermore, two different base patterns were used, square or hexagonal pattern. A constant height of 15 μm was fixed for all the pillar topologies Fig. 2.

Surface texturing introduces hierarchical substructures in the post structures. A textured surface is obtained by a TMAH solution, which etches the silicon with a high selectivity on the crystalline planes. Hence, by using a ⟨1 0 0⟩ silicon wafer, a heterogeneous and compact pattern of pyramid-like pillars was obtained [12]. The base angle of the pyramid is equal to 54.7°, which corresponds to the angle between ⟨1 1 1⟩ and ⟨1 0 0⟩ planes. The texturing process is composed of two steps; firstly a dip in buffered hydrofluoric acid (BHF) is needed to completely remove the native oxide on the silicon substrate, then a 5 min wet etch in the TMAH 2% solution is performed; this process can be considered as the hierarchical module. Combining the hierarchical module and the base process module it is possible to generate two different structures, as shown in Fig. 3. In particular, it is possible to obtaine a pillar with only the upper part texturized (Fig. 3a) or to extend the texturing on the entire structure (Fig. 3b), thus including the lateral sides. Due to the presence of a thin native SiO_2 layer, which makes the silicon surface naturally hydrophilic, a self-assembly monolayer (SAM) coating is needed to impose hydrophobicity [13]. In particular,

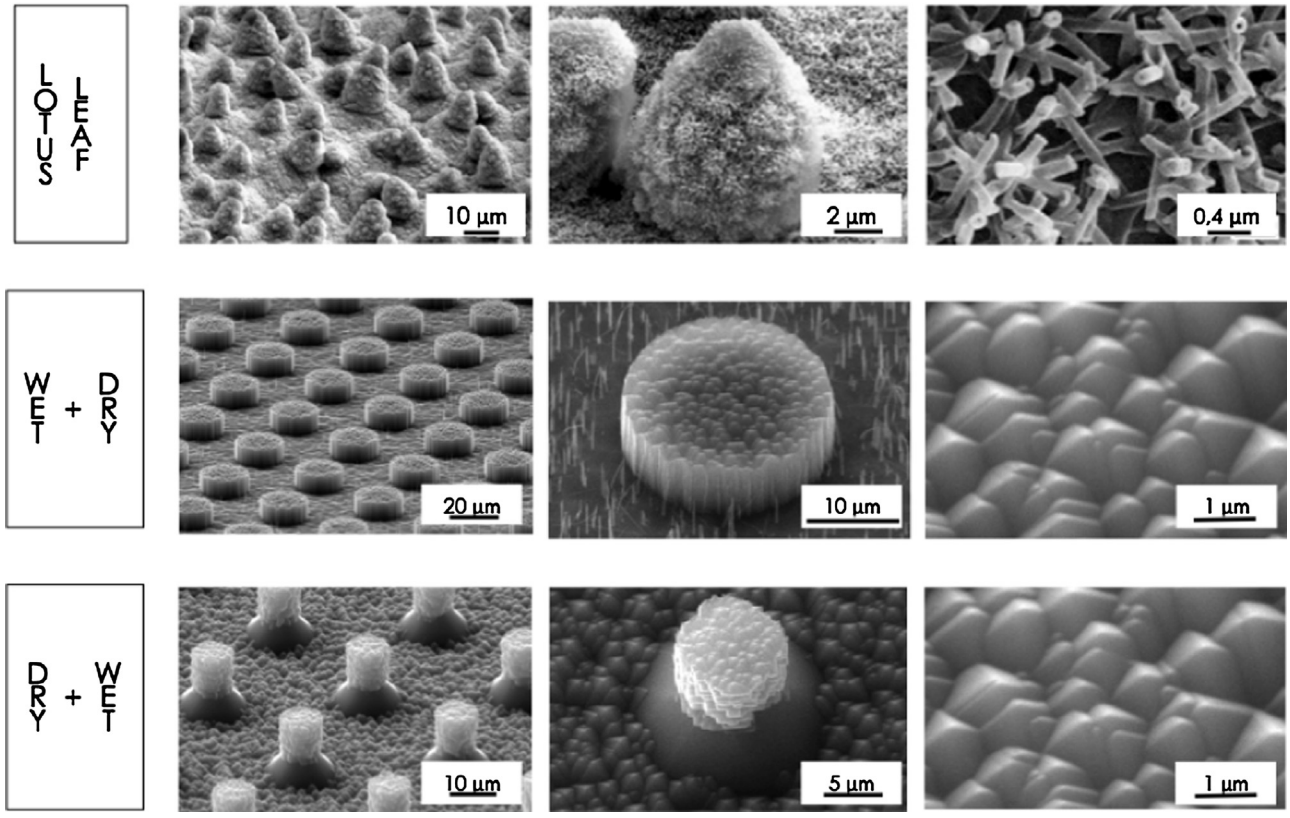

Fig. 2. Surface topologies generated with the two processes and compared with the lotus leaf (image of lotus leaf from reference [5]).

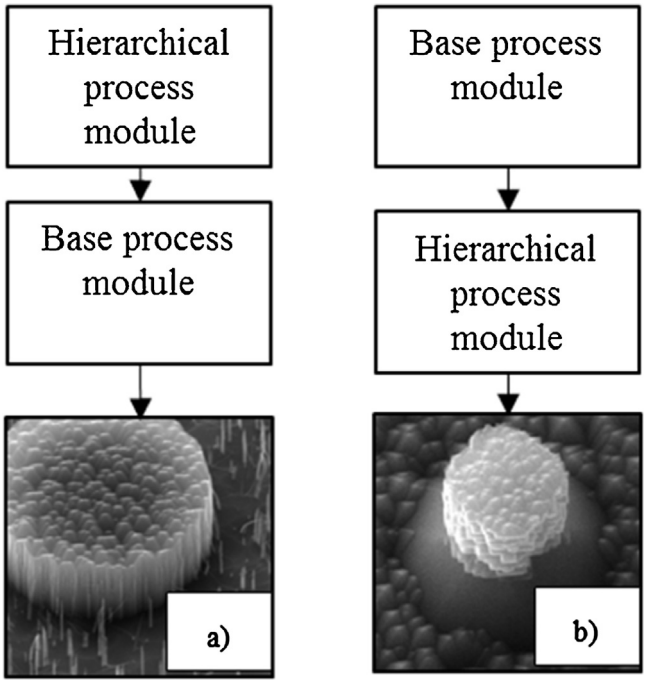

Fig. 3. Schematic description of the two processes to generate the hierarchical structures: (a) wet plus dry process and (b) dry plus wet process.

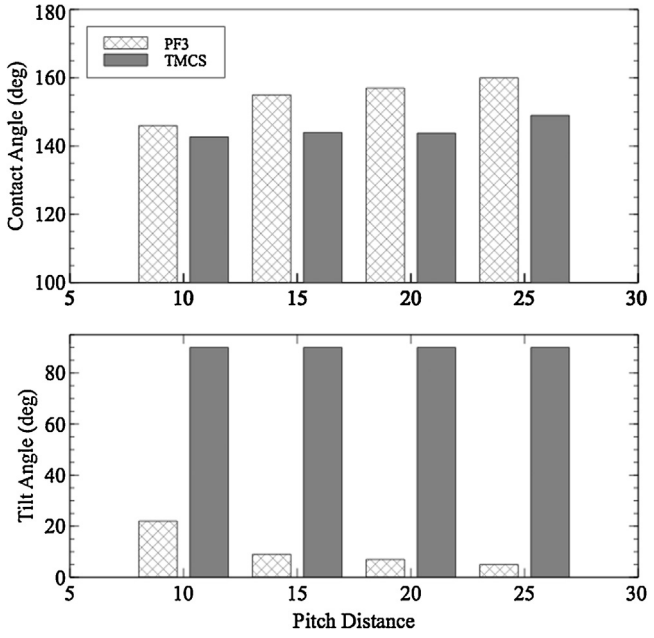

Fig. 4. Contact and tilt angle measurements of structures with post diameter of 10 μm and different pitch distances (microns). Graphs show the comparison between the two types of coatings, i.e., PF3 or TMCS. Conventionally here 90° denotes the sticky condition.

Trimethylchlorosilane (TMCS) and 1-1-2-2-perfluorodecyltrichlorosilane (PF3) were used for SAM vapor/phase deposition [13].

2.2. Wettability analysis

Wettability measurements were performed using 5 μl drops of deionized water (18 MΩ of resistance). An estimation of drop contact angle was calculated using "drop analysis" software [14]. Experimental results are reported in the next section.

2.2.1. Non-hierarchical pillars

In this section surfaces patterned with pillars, of different diameters and pitch distances, are analysed and compared.

The first results, shown in Fig. 4, refer to a comparison between the two different coatings; PF3 has better performance than TMCS.

PF3 coatings renders silicon oxide substrates hydrophobic (CA = 109°) in contrast to TMCS coatings (CA = 78°) [8,15]. However, TMS is quite easy to deposit on the silicon substrate, e.g. the process occurs at room temperature in a closed chamber, while PF3 deposition requires a more complex process, e.g., a well-controlled temperature [13]. Surfaces coated with TMCS in general display an increment of their contact angle, showing Cassie–Baxter interface even if the substrate is intrinsically hydrophilic.

The graphs in Fig. 4 provide results of contact or tilt angles for structures coated with TMCS and PF3, respectively. The structures considered have post diameter of 10 μm and pitch distances between 15 and 30 μm.

Charts on Fig. 4 show that not only the contact angle is better for PF3 coating with respect to TMCS coating, but especially the tilt angle. Indeed, TMCS results in a sticky condition, represented in the graph with value of tilt angle equal to 90°, while surfaces coated with PF3 have low tilt angle. For these surfaces the tilt angle decreases as the pitch distance increases. For these reasons all surfaces considered in this work were coated with PF3.

In order to better understand the role of pattern geometries on the surface wettability, square or hexagonal base patterns were

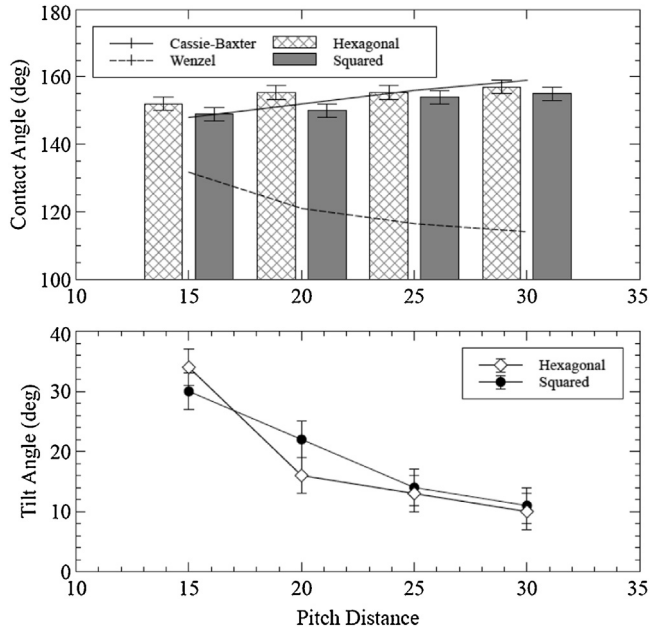

Fig. 5. Contact and tilt angle measurements and predictions of structures with post diameter of 10 μm and different pitch distances (microns): comparison between square and hexagonal base patterns.

generated and analysed. A whole series of structures with pillars of different diameters and different pitch distances were examined. Graphs in Fig. 5 show the trend of contact and tilt angles for the two patterns: no significant difference is observable.

In addition Fig. 5 presents two analytical predictions for contact angle, where continuous black or dotted lines represent the Cassie–Baxter [16] and the Wenzel [17,18] predictions respectively. After comparison between analytical predictions and experimental data, it is possible to deduce that surfaces stand in Cassie–Baxter state. Stability of this state has been discussed in Section 3.1.

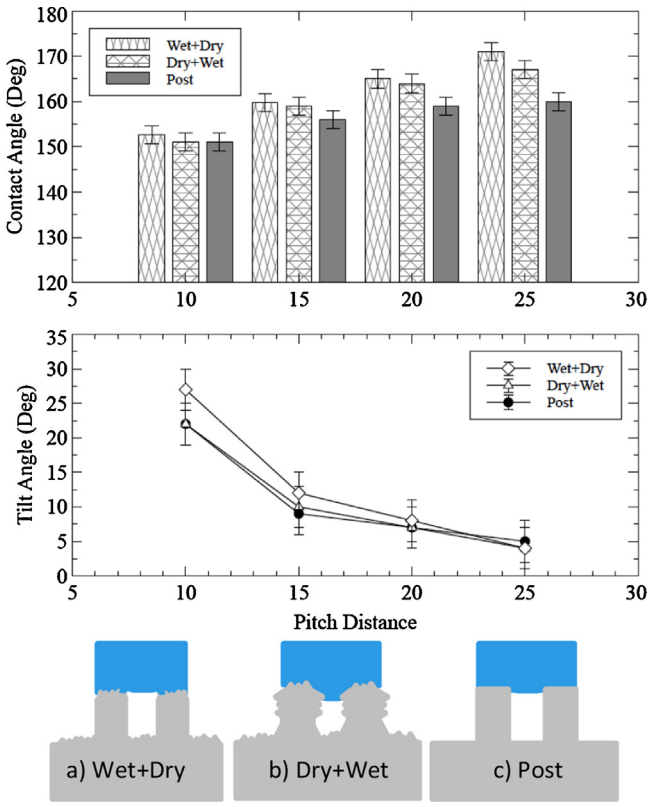

Fig. 6. Contact and tilt angle measurements of structures with post diameter of 5 μm and different pitch distances; comparison between the two hierarchical structures (a) wet + dry (b) dry + wet and the non-hierarchical one (c).

2.2.2. Hierarchical pillars

In this section similar analyses conducted on the non-hierarchical structures are performed on hierarchical ones (Fig. 6 shows below the graphs a sketch of the different structures). Two kinds of hierarchical structures were developed, as illustrated in Fig. 6a and b. The wet plus dry process generates structures similar to those reported in Fig. 6a whereas the dry plus wet process to those reported in Fig. 6b. These structures were tested for both contact and tilt angles.

In Fig. 6, comparisons between two kinds of hierarchical structures and one kind of pillar structure are reported. Considering surfaces with pillars of 5 μm, four different pitch distances were compared, from 10 μm up to 20 μm. The results reported in Fig. 6 refer to those surfaces which reach highest contact angles and lowest tilt angles. During this study, diameters of 5, 10, 15 and 20 μm were analysed and rationalized according to the Cassie–Baxter equation. The surfaces with a lower solid–liquid interface area fraction φ have a greater contact angle, as is the case of pillars with smaller diameters.

Fig. 6 also shows how both hierarchical structures present a significant improvement with respect to the post structures in terms of contact angle. Tilt angle varies with the pitch distance for both hierarchical and post structures.

It has been discussed how hierarchy improves the contact angle, however tilt angle does not change significantly with the introduction of a hierarchical level. In some cases, the introduction of an additional level seems almost counter-productive, as can be observed in Fig. 6 for the lower pitch distance. This can be due to the partial impalement of the drop on the textured surface, as discussed in the next section.

Table 1
Minimum intrinsic contact angle (degrees) to achieve stable Cassie–Baxter states for different pitch distances (columns) and pillar diameters (rows), measured in microns.

	10	15	20	25	30	35	40
5	104.7	117.8	128.1	136.0	–	–	–
10	–	103.7	113.9	122.5	129.5	–	–
15	–	–	103.9	112.8	120.4	126.7	–
20	–	–	–	104.4	112.5	119.4	125.2

3. Theoretical analysis

In this section, analytical models are implemented in order to validate the experimental results and consider the stability of the experimental state. Classical theories of Wenzel [17,18] and Cassie–Baxter [16] are used to fit experimental data for non-hierarchical structures. A general model, combining Cassie–Baxter and Wenzel theories and taking into account hierarchy, is presented following the hierarchical theory proposed by Pugno [5,6].

3.1. Non-hierarchical pillars

It is a straightforward analysis to compute the predictions of the two classical models for surfaces with non-hierarchical pillars, where roughness and area fraction values can be deduced geometrically. Roughness r for a patterned surface is expressed in Eq. (1), while the solid-liquid area fraction is defined by Eq. (2), in which P is the pitch distance, H is the pillar height and d is the pillar diameter.

$$r = \frac{A_{\text{real}}}{A_{\text{projected}}} = 1 + \frac{\pi d H}{P^2} \tag{1}$$

$$\varphi = \frac{A_{\text{solid-liquid}}}{A_{\text{total}}} = \frac{\pi d^2}{4P^2} \tag{2}$$

It is useful for our purpose to split Eq. (1) in Eqs. (3) and (4). In particular Eq. (3) shows the increase of the effective area due to the lateral sides of the pillars, while Eq. (4) describes the ratio between the area on top and bottom of pillars and the projected area; for definition this ratio is equal to one, namely:

$$r_L = \frac{A_{\text{Lateral}}}{A_{\text{projected}}} = \frac{\pi d H}{P^2} \tag{3}$$

$$r_{TB} = \frac{A_{\text{Top}} + A_{\text{Bottom}}}{A_{\text{projected}}} = \frac{P^2}{P^2} = 1 \tag{4}$$

Then it is straightforward to define $r = r_L + r_{TB}$.

Experimentally drops on the surfaces appear in Cassie–Baxter state, as can be deduced by comparing experimental results with analytical predictions, Fig. 5. This state is stable if Eq. (5) is true [19] for the intrinsic contact angle ϑ_0:

$$\cos\vartheta_0 < \frac{\varphi - 1}{r - \varphi} \tag{5}$$

Table 1 shows the minimum value of intrinsic contact angle at which the structure has a stable Cassie–Baxter interface for the corresponding geometrical parameters. The surface base contact angle for the PF3 coating is $\vartheta_0 = 109^\circ$. It can be seen that most of the structures analysed are theoretically not stable in Cassie–Baxter configuration. However, secondary effects generate an energy barrier between the Cassie–Baxter and Wenzel state, rendering the first metastable rather than unstable [20], as observable in our experiments.

3.2. Hierarchical pillars

The wetting state becomes more difficult to predict for hierarchical structures. Indeed, hierarchical surfaces can have more

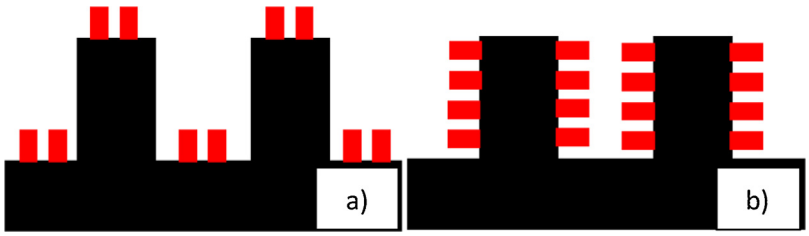

Fig. 7. Sketches of the fabricated hierarchical structures (a) with hierarchy on the top and bottom of the pillars and (b) with hierarchy only on the lateral side of the pillars. For interpretation of the references to colour in the text, the reader is referred to the web version of this article.

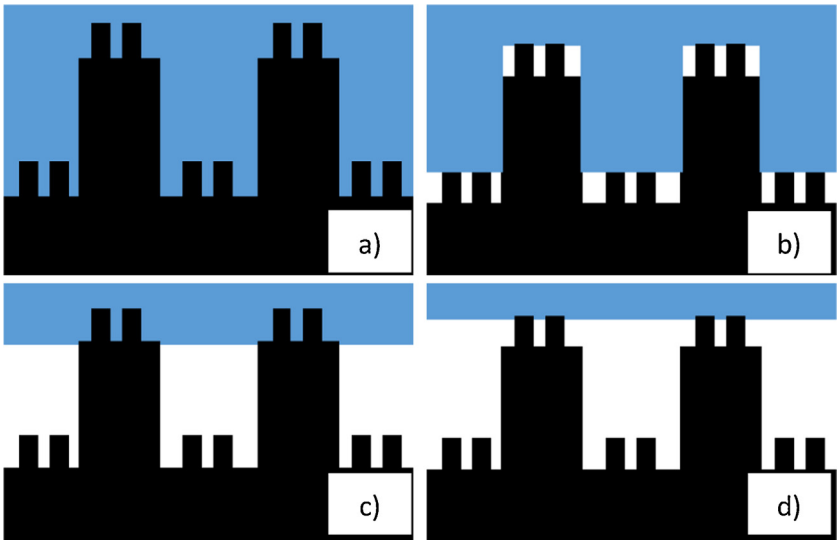

Fig. 8. Different wetting states of hierarchical structures of type 1: (a) complete wetting or Wenzel state, (b) Wenzel state on the surface and Cassie–Baxter state on the pillars, (c) Cassie–Baxter state on the surface and Wenzel state on pillars, (d) complete Cassie–Baxter state.

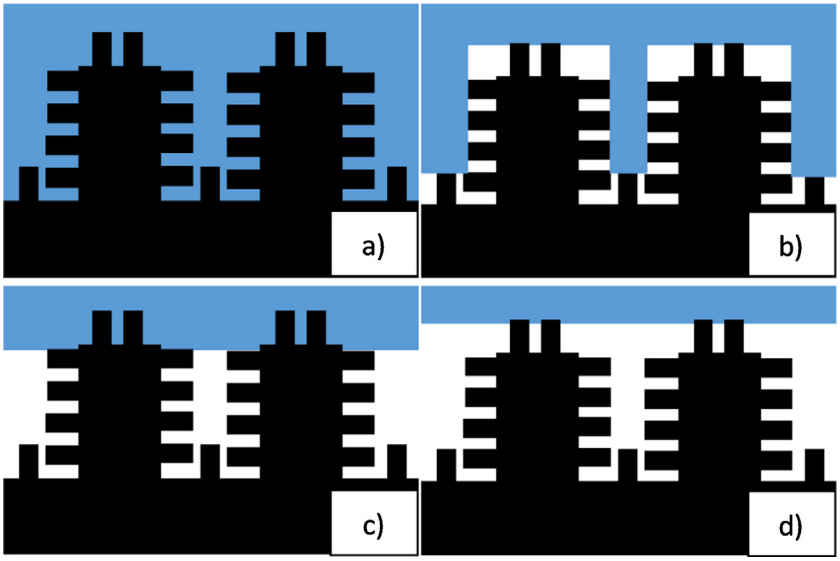

Fig. 9. Different wetting states of hierarchical structures of type 2: (a) complete wetting or Wenzel state, (b) Wenzel state on the surface and Cassie–Baxter state on the pillars, (c) Cassie–Baxter state on the surface and Wenzel state on pillars, (d) complete Cassie–Baxter state.

complex interfaces. Typical examples of a complex natural interface is that of the rose petals [21]. Two different hierarchical structures are considered here: one with hierarchy on the top and the bottom of the pillars, Fig. 7a, and one with hierarchy only around the lateral side of the pillars, Fig. 7b. More complex structures, as shown in Figs. 8 and 9, can be easily manufactured with our process. Fig. 8 is a schematic representation of the wet plus dry process, while Fig. 9 represents the surface generated with dry plus wet process. The roughness parameter and area fraction can again be found with geometrical considerations for both cases, allowing the analysis of different kinds of hierarchical structures thanks to equations from (6) to (9).

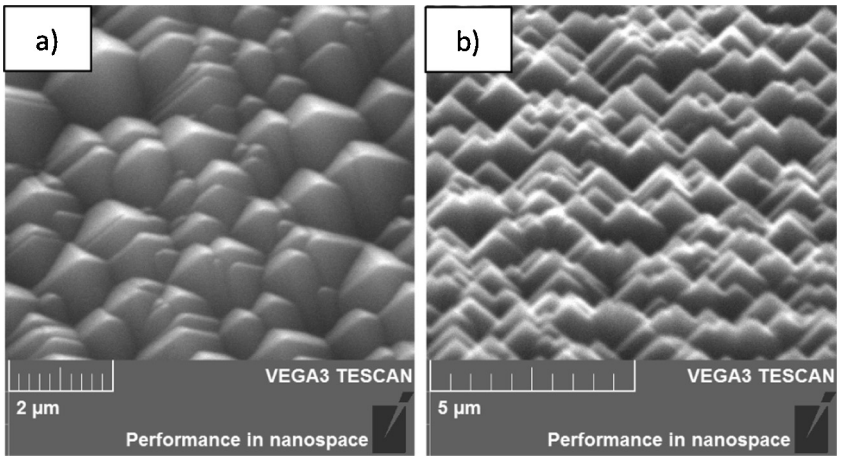

Fig. 10. (a) Top view of silicon textured surface after five minutes of TMAH. (b) 70° tilted view of silicon textured surface.

Eqs. (6) and (7) describe the area fraction and the roughness parameter for the first order level hierarchical structures, i.e. (red) sub-pillars in Fig. 7a:

$$\varphi_g = \frac{\pi d'^2}{4p^2} \tag{6}$$

$$r_g = 1 + \frac{\pi d' h}{p^2} \tag{7}$$

where d', h, and p are diameter, height and pitch distance of the sub-pillars. Similarly, to describe the hierarchical structures in Fig. 7b, we obtain geometrically:

$$\varphi_l = \frac{\pi d'^2}{4p^2} \tag{8}$$

$$r_l = 1 + \frac{\pi d' h}{p^2} \tag{9}$$

With the two hierarchical levels experimentally considered, four different wetting configurations are possible for each structure, Figs. 8, 9. Each configuration represents a combination of Wenzel and Cassie–Baxter states at different hierarchical levels, where the first letter of the subscript indicates the state of the base level and the second letter indicates the state of the hierarchical level, W stand for Wenzel state and C for Cassie–Baxter state. Stable configuration will be the one with lower energy, for non-hierarchical surfaces this is the state with lower contact angle. In the following section the equations that predict contact angles in the different wetting configurations are presented. Following [5] each wetting state shown in Figs. 8 or 9 is described by equations from (10) to (13), corresponding respectively to the contact angles denoted by ϑ_{ww}, ϑ_{wc}, ϑ_{cw}, and ϑ_{cc}.

$$\cos\vartheta_{ww} = r_L r_l \cos\theta_0 + r_{TB} r_g \cos\theta_0 \tag{10}$$

$$\cos\vartheta_{wc} = r_L\left(\varphi_l\left(\cos\theta_0 + 1\right) - 1\right) + r_{TB}(\varphi_g(\cos\theta_0 + 1) - 1) \tag{11}$$

$$\cos\vartheta_{ww} = r_L r_l \cos\theta_0 + r_{TB} r_g \cos\theta_0 \tag{12}$$

$$\cos\vartheta_{cc} = \varphi\varphi_g\left(\cos\theta_0 + 1\right) - 1 \tag{13}$$

Eqs. (10) and (11) are valid for the general case of hierarchical surfaces. It is possible to apply them for our surfaces in Figs. 8 or 9 by imposing respectively $r_l = 1$ or $\varphi_l = 1$. Eqs. (12) and (13) are valid for both kind of surfaces [5,6]. Furthermore it can be seen that Eq. (13) was already studied as a particular case of Cassie–Baxter equation [16].

3.2.1. Computing the area fraction φ for pyramidal pillars

Our fabricated pillars are nearly square-base pyramidal elements, see Fig. 10. Physical dimensions of the tips are not easily calculable, giving rise to problems on computing the area fraction for such a surface.

The monocrystalline structure of the silicon substrate and the high selectivity of the TMAH etch to the crystalline plane leads to a base angle for each pyramidal element of $\alpha = 54.7°$ [12]. The roughness parameter, define as the ratio between surface area and projected area, is for overlapping pyramidal elements, as in our case (Fig. 10), only a function of the base angle, geometrically:

$$R = \frac{1}{\cos\alpha} \tag{14}$$

This fixed value of roughness allow us to predict the apparent contact angle of the textured surfaces in Wenzel state as $\vartheta_w = 124.3°$.

The Cassie–Baxter equation would predict an apparent contact angle of $\vartheta_{CB} \cong 180°$, as the drop is just posed on the top of the pyramidal elements and the area fraction would tend to 0. This situation is described in the following equation:

$$\cos\vartheta_{CB} = \varphi(\cos\vartheta_0 + 1) - 1 \to -1, \tag{15}$$

$$if \quad \varphi \to 0$$

Between these two limits, Eq. (16) describes the trend of the apparent contact angle with variable area fraction:

$$\cos\vartheta_{\mathrm{Mix}} = \varphi(z)(R\cos\vartheta_0 + 1) - 1 \tag{16}$$

as can be deduced by Eq. (12).

We define z as the distance between the water surface and the bottom of the pyramidal elements, so that when $z = 0$, the system is in the Wenzel state, whereas when $z = h_{max}$ the related hierarchical level is in the Cassie–Baxter state.

Experimentally, the contact angle of the texturized surface is $\vartheta_{\mathrm{Mix}} = 135°$. Inserting this value in Eq. (16) it is possible to calculate the value of the area fraction. For this configuration the area fraction is $\varphi(z) = \varphi_{\mathrm{Mix}} = 0.67$. This value can be used as reference value also in the other Eqs. (10–13). Thus the area fraction value for the hierarchical level is $\varphi_l = \varphi_g = \varphi_{\mathrm{Mix}} = 0.67$. Similarly the roughness parameters are $r_l = r_g = R$.

4. Results and discussion

Predictions of contact angles are done inserting the previous values into Eqs. (10)–(13).

Table 2
Predicted values of contact angle (degrees) compared with experimental data for structures (microns × microns) and configurations of Fig. 8.

Diameter × pitch	θ_{ww}	θ_{wc}	θ_{cw}	θ_{cc}	Exp. data
5 × 10	180.0	180.0	156.1	155.7	160.6
5 × 15	154.7	180.0	155.9	160.3	161.9
5 × 20	139.0	180.0	162.0	165.3	164.0
5 × 25	133.3	180.0	165.6	168.2	171.1

Table 3
Predicted values of contact angle (degrees) compared with experimental data for structures (microns × microns) and configurations of Fig. 9.

Diameter × pitch	θ_{ww}	θ_{wc}	θ_{cw}	θ_{cc}	Exp. data
5 × 10	180.0	180.0	156.1	155.7	160.0
5 × 15	180.0	180.0	155.9	160.3	158.9
5 × 20	153.5	180.0	162.0	165.3	164.8
5 × 25	140.9	180.0	165.6	168.2	167.3

Table 2 shows the predicted contact angle for structures without lateral texturing (of Fig. 8). Different structure geometries are analysed and compared with experimental data.

Non-hierarchical theory shows that the most stable configuration is the one corresponding to the lower contact angle. Hence, the stable states are expected to be described by θ_{cc}, θ_{cw} and θ_{ww}, depending on the geometries. However, experimental data seem to follow the prediction of θ_{cc} even when it is not the most stable state. This behavior can be explained by the presence of an energy barrier that does not allow the transition from Cassie–Baxter to Wenzel state [22]. The drop is then in a metastable state for these geometries.

Table 3 shows the prediction of contact angles for the surfaces with hierarchy also on the lateral side (of Fig. 9), whereas on the rightmost column the experimental data are shown.

Similar considerations valid for the data in Table 2 also apply for those reported in Table 3. In fact, the experimental data are quite similar for the two hierarchical configurations. However, the hierarchical configuration with no texturing on the lateral surfaces, Fig. 8, displays a higher contact angle. This phenomenon could be explained as an increasing of the effective upper area due to the presence of the first ring of lateral textured surfaces. Analytical results have shown how the state corresponding to θ_{cc} increases its stability range with respect to that described by θ_{ww} thanks to the presence of the lateral texturing.

From these analyses it is possible to conclude that the experimental results for both hierarchical and non-hierarchical structures can be validated via the presented hierarchical theory [5,6]. Furthermore all the states seem to be metastable Cassie–Baxter configurations.

5. Conclusion

In this paper, a new process to quickly generate large superhydrophobic surface areas composed of hierarchical structures has been presented. By changing the steps order inside the process it is possible to generate two different kinds of structures: patterns with different hierarchical geometries were generated using the two processes. Furthermore, patterns without hierarchy were also generated as references.

All the surfaces were tested for hydrophobicity, and hierarchical structures show a significant improvement of their non-wettability properties with respect to the non-hierarchical ones. Experimental results have been rationalized by applying Wenzel and Cassie–Baxter classical equations extended to consider hierarchy as proposed by Pugno [5,6].

Both hierarchical structures show higher contact angles with respect to non-hierarchical structures. The best result shows a contact angle equal to 171° and a tilt angle of 4°, outperforming the wettability of a real lotus leaf. It has been observed for the wet plus dry process with pillar diameter of 5 μm and pitch distance of 25 μm at a production rate of about 90 min per silicon wafer, which leads to an approximate rate of 30 s/cm^2. Although the best result for tilt angle was obtained from the same surface, it is not possible to deduce significant differences on it between hierarchical and non-hierarchical surfaces.

This fast and effective method could pave the way to large scale production of lotus-inspired superhydrophobic surfaces.

References

[1] W. Barthlott, C. Neinhuis, Purity of the sacred lotus, or escape from contamination in biological surfaces, Planta 202 (1997) 1–8.
[2] C. Neinhuis, W. Barthlott, Characterization and distribution of water-repellent, self-cleaning plant surfaces, Ann. Bot. 79 (1997) 667–677.
[3] E. Lepore, et al., Plasma and thermoforming treatments to tune the bio-inspired wettability of polystyrene, Composites Part B 43 (2012) 681–690.
[4] E. Lepore, N. Pugno, Superhydrophobic polystyrene by direct copy of lotus leaf, BioNanoSci. 1 (2011) 136–143.
[5] N. Pugno, Mimicking lotus leaves for designing super-hydrophobic/hydrophilic and super-attractive/repulsive hierarchical nanostructured surfaces, Nanomechanics in Italy (2007) 1–9.
[6] N. Pugno, Towards a Spiderman suit: large invisible cable and self-cleaning releasable superadhesive materials, J. Phys.: Condens. Matter 19 (2007) 395001.
[7] S. Yewang, et al., Nano to micro structural hierarchy is crucial for stable superhydrophobic and water-repellent surfaces, Langmuir 26 (2010) 4984–4989.
[8] B. Bhushan, et al., Micro-, nano- and hierarchical structures for superhydrophobicity, self-cleaning and low adhesion, Phil. Trans. R. Soc. A 367 (2009) 1631–1672.
[9] B. Bhushan, Y.C. Joung, Natural and biomimetic artificial surfaces for superhydrophobicity, self-cleaning, low adhesion and drag reduction, Progress Mater. Sci. 56 (2016) 1–108.
[10] K. Koch, et al., Chemistry and crystal growth of plant wax tubules of lotus and nasturtium leaves on technical substrate, Cryst. Growth Des. 6 (2006) 2571–2578.
[11] B. Bhushan, Biomimetics inspired surfaces for drag reduction and oleophobicity/philicity, Beilstein, J. Nanotechnol. 2 (2011) 66–84.
[12] P. Papet, et al., Pyramidal texturing of silicon solar cell with TMAH chemical anisotropic etching, Solar Energy Mater. Solar Cells 90 (15) (2006) 2319–2328.
[13] T. Kasai, B. Bhushan, G. Kulik, Barbieri, L. Hoffmann, Micro/nanotribological study of perfluorosilane SAMs for antistiction and low wear, J. Vac. Sci. Technol. 23 (2005) 995–1003.
[14] Y.C. Jung, B. Bhushan, Wetting transition of water droplets on superhydrophobic patterned surfaces, Scr. Mater. 57 (2007) 1057–1060.
[15] A.B.D. Cassie, S. Baxter, Wettability of textured surfaces, Colloids Surf. 40 (1944) 546–551.
[16] F. Stalder a, G. Kulik, D. Sage, L. Barbieri, P. Hoffmann, A snake-based approach to accurate determination of both contact points and contact angles, Colloids Surf. A 286 (1–3) (2006) 92–103.
[17] R.N. Wenzel, Resistance of solid surfaces to wetting by water, Ind. Eng. Chem. 28 (1936) 988–994.
[18] R.N. Wenzel, Surface roughness and contact angle, J. Phys. Chem 53 (1949) 1466–1470.
[19] J. Bico, U. Thiele, D. Quèrè, Wetting of textured surfaces, Colloids Surf. 206 (2002) 41–46.
[20] D. Quèrè, Non-sticking drops, Rep. Prog. Phys. 68 (2005) 2495–2532.
[21] B. Bhushan, M. Nosonovsky, The rose petal and the modes of superhydrophobicity, Phil. Trans. R. Soc. 368 (2010) 4713–4728.
[22] M. Nosonovsky, B. Bhushan, Stochastic model for metastable wetting of roughness-included superhydrophobic surfaces, Microsyst. Technol. 13 (2006) 231–237.